Proceedings of Proceedings of the ASME 2014 4th Joint US-European Fluids Engineering Division Summer Meeting and 11th International Conference on Nanochannels, Microchannels, and Minichannels
FEDSM2014
August 3-7, 2014, Chicago, Illinois, USA

DRAFT: FEDSM2014-22172

INFLUENCE OF DESIGN PARAMETERS ON THE GLOBAL PERFORMANCES OF LOW-SPEED COUNTER-ROTATING AXIAL-FLOW FANS

Juan WANG
Dynfluid Laboratory
Arts et Metiers ParisTech
Paris, France
juan.wang@ensam.eu

Florent RAVELET
Dynfluid Laboratory
Arts et Metiers ParisTech
Paris, France
florent.ravelet@ensam.eu

Farid BAKIR
Dynfluid Laboratory
Arts et Metiers ParisTech
Paris, France
farid.bakir@ensam.eu

ABSTRACT

The present work aims at experimentally investigating the effects of some parameters on the performances of a counter-rotating stage, and on the instationary flow between the rotors. Three counter-rotating fans, which have the same design point, have been designed. These systems differ by the distribution of the loading and of the ratio of angular velocity between the front rotor and the rear rotor. All the configurations have been tested in a normalized test rig, where the ratio of angular velocities and the axial distance between the two rotors can be varied. The influence of these parameters are then addressed by analysing the experimental results of the static pressure rise and static efficiency, as well as of the wall pressure fluctuations registered by a microphone at the wall. The three systems achieve the design point with a high efficiency. The counter-rotating systems lead to at least a 10 percentage points gain in static efficiency at the design flow rate, compared to the typical peak efficiency of a traditional rotor-stator stage. Meanwhile, counter-rotating systems display good working stabilities at very low volume flow rates. In addition, at the design speed ratio, the overall performance decreases almost monotonically with the axial distance. Nevertheless, an optimum in axial distance can be found for higher speed ratios. Finally, the investigations of the wall pressure fluctuations show that the amplitudes of power spectral density corresponding to the blade passing frequency of the rear rotor are significantly higher than that of the front rotor. The interaction peaks are also stronger for an equal distribution of the work on the two rotors.

NOMENCLATURE

ΔP_t Total pressure rise (Pa)
ΔP_s Static pressure rise (Pa)
D Pipe diameter (mm)
Q_v Volume flow rate ($m^3.s^{-1}$)
R_{tip} Blade tip radius(mm)
R_{hub} Blade hub radius (mm)
N Rotational speed of rotor (rpm)
θ Rotational speed ratio $\frac{N_{RR}}{N_{FR}}$
L Distribution of load $\frac{\Delta P_{t,RR}}{\Delta P_{t,FR}+\Delta P_{t,RR}}$
Z Number of blades
P_w Power consumption of the rotor (W)
Z_p Axial position of microphone
S Axial distance between front rotor and rear rotor (mm)
L_{chord} Blade chord (mm)
W Relative velocity ($m.s^{-1}$)
U Rotor velocity ($m.s^{-1}$)
C_a Axial velocity ($m.s^{-1}$)
p' Wall pressure fluctuation (Pa)
γ Stagger angle
ρ_a Density of air ($kg.m^{-3}$)
τ torque (N.m)
μ Dynamic viscosity of the fluid (Pa.s)

FR Front Rotor
RR Rear Rotor
CRS Counter Rotating System
C Conception

1 INTRODUCTION

Adoption of a counter-rotating machine has opened a way to design high performance and compact turbomachines in various industrial domains. It has been already applied in the areas of subsonic fans, pumps and turbines [1–3]. A Counter-Rotating System (CRS) is composed of a Front Rotor (FR) and a Rear Rotor (RR) which rotates in the opposite direction, as shown in Fig. 1. Compared with traditional rotor-stator system, the Rear Rotor is used not only to recover the static head but also to supply energy to the fluid. Therefore, to achieve the same performance, the use of a CRS may lead to a reduction of the rotational speed and may generate better homogeneous flow downstream of the stage.

On the other hand, the mixing area in between the two rotors induces complicated interacting flow structures. The understanding of this highly unsteady flow in the mixing area is an open problem. Moreover, the design method of such machines is still not sophisticated, due to a lack of systematic studies on the influence of free parameters, such as the distribution of load (L), the axial distance (S), the ratio of the rotation rates (θ) and so on...

In the Dynfluid Laboratory, series of experiments focused on axial counter rotating fans have been performed [4]. Based on this research, three CRS (JW1, JW2 and JW3) have been designed to attain the same design point, while varying the distribution of load. The main concern in this paper is the influence of the distribution of load (L) on the overall performances of a CRS.

The conception of the three CRS and their design parameters are presented in Section 2. Then the experimental facility, the measurement method and the analysis of uncertainty as well as repeatability are presented in Section 3. The results are presented in Section 4. The overall performances for the nominal S and θ are first presented in § 4.1, then the influence of the axial distance and of the variation of θ are discussed for each CRS, in respectively § 4.2 and § 4.3. In addition, the levels and spectral densities of the wall pressure fluctuations in the mixing area between the front and rear rotors are compared in § 4.4.

2 DESIGN OF THE COUNTER-ROTATING FANS SYSTEMS

2.1 Methodology

The objective is to design three CRS which can achieve the same design point for various distributions of the total load between the front and rear rotors. The design point is presented in

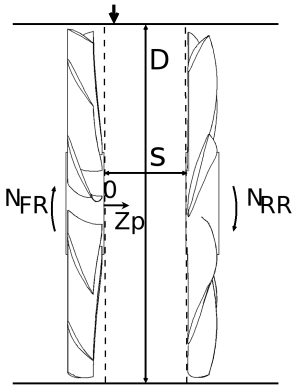

FIGURE 1. Sketch of the CRS. The bold arrow stands for the microphone (position $Z_p = 5$ mm downstream the front rotor).

D (mm)	R_{tip} (mm)	R_{hub} (mm)	ΔP_{tC} (Pa)	Q_{vC} ($m^3.s^{-1}$)
380	187.5	65	420	1

TABLE 1. Design point for air at $\rho_a = 1.21$ kg.m^{-3}.

Tab. 1. In this table, the total pressure rise is the difference of *total pressure* between the inlet and the outlet of the CRS. One of the design constraint is to have a pure axial flow downstream of the CRS. Therefore, the corresponding expected *static* pressure rise is calculated as $\Delta P_{sC} = \Delta P_{tC} - \frac{1}{2}\rho_a(\frac{Q_{vC}}{\pi D^2/4})^2 \approx 373$ Pa.

With this in mind, firstly, the front rotor was designed to achieve a part of the total pressure rise at design flow rate, by the in-house code MFT [5]. The details of the conception method can be found in Ref. [4]. The outlines could be depicted as follows: the geometrical parameters of the Front Rotor are designed by MFT with the inverse method. Then the axial and tangential velocities at the outlet of the Front Rotor are analysed and taken as the input conditions for the conception of the Rear Rotor. Therefore, the Rear Rotor is adapted to the outflow of the Front Rotor, and is designed such that the absolute tangential velocity at the outlet of the system vanishes.

2.2 Characteristics of the three different CRS

The main parameters can be found in Tab. 2 and Fig. 2. The distribution of load is defined as the ratio of the total pressure rise due to the Rear Rotor to that of the Counter-Rotating System at the design flow rate: $L = \frac{\Delta P_{t,RR}}{\Delta P_t}$. All the three CRS have different L at the same design point. The Front Rotors of the three systems are designed with the same blade loading repartition, with a "Constant Vortex" Design (see Refs. [6, 7]). The peculiar features of each system are the following:

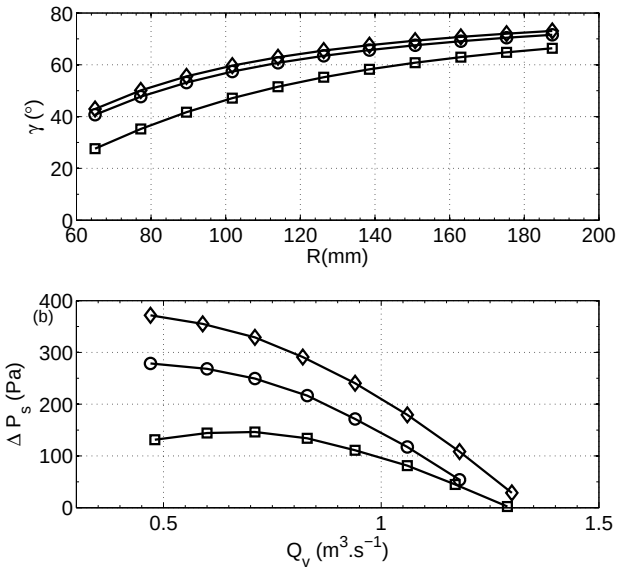

FIGURE 2. Conception by MFT [5] of $JW1_{FR}$ (○); $JW2_{FR}$ (□) and $JW3_{FR}$ (◊). (a): radial profile of the stagger angle and (b): static pressure rise calculated by a semi-empirical model [5].

JW1. The Front Rotor of JW1 ($JW1_{FR}$) is designed to have large stagger angles, in order to obtain a steep curve of static pressure rise ΔP_s as a function of the volume flow rate Q_v (see Fig. 2). Aside from this, the other parameters (rotation rates and ratio θ) are very similar to those of the configuration that was studied in Ref. [4].

JW2. Among the three CRS, JW2 has the highest $L = 52\%$, that is to say, in this Counter-Rotating System, the Rear Rotor transfers more energy to the fluid than the Front Rotor. Consequently, the Front Rotor $JW2_{FR}$ possess the lowest ΔP_s among the three Front Rotors. It is furthermore designed with low stagger angles and has a slowly decaying characteristics (see Fig. 2). The Rear Rotor rotates 1.44 times faster than the Front Rotor in that configuration.

	N_{FR}/N_{RR} (rpm)	θ_C	L %	Z_{FR}/Z_{RR}	γ_{FR}
JW1	2300/2200	0.96	41	10/7	large
JW2	1800/2600	1.44	52	13/7	small
JW3	2600/1100	0.42	23	10/7	large

TABLE 2. Design parameters of the three CRS.

JW3. This is an extreme case where $JW3_{FR}$ leads to the highest and steepest characteristics, as shown in Fig. 2. As a result, JW3 has the lowest $L = 23\%$ among the three configurations, and the Rear Rotor rotates much more slowly than the Front Fotor.

Finally, please note that since the Rear Rotors are designed to rectify the outflow of the Front Rotors toward the axial direction, the shape of the Rear Rotors that are obtained is not usual, with non-monotonic stagger angle and blade camber profiles (see Fig. 3 for an example on $JW1_{RR}$).

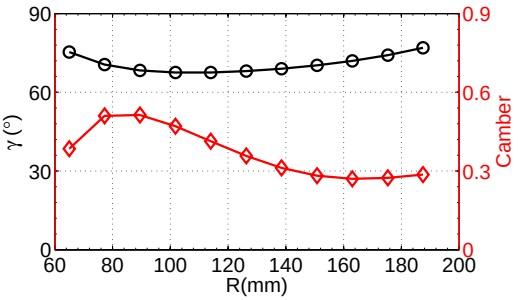

FIGURE 3. Radial profiles of the stagger angle (○) and of the aerodynamic camber (◊, see Ref. [7] for a definition) for the rotor $JW1_{RR}$.

3 EXPERIMENTAL FACILITIES

3.1 Test rig

The experimental investigation are performed in a test rig, built according to the ISO-5801 standard. First, the air comes into the test pipe of diameter $D = 380$mm trough a bell mouth, then passes through the driving motor of the Front Rotor, and is homogenized by a honeycomb. Next, energy is transferred to the fluid by the two rotors. They are separated by a series of blocks for the purpose of varying the axial distance S between them. Then, the outflow passes the driving motor of the Rear Rotor and an anti-gyration device to remove the rotational component of the flow before the measurement of the static pressure by 4 pressure taps. After that, the fluid goes through an ISO-5167 orifice plate in order to measure the volume flow rate (Q_v). Finally, the fluid is regulated by an axial blower and an iris damper before being discharged into the ambient atmosphere.

3.2 Experimental method and Estimation of the uncertainties

The uncertainty are first estimated according to the repeatition of measurements at the design point. Specifically, ten measurements have been performed at the same rotation rates and for a fixed diameters of the iris damper.

Density of air ρ_a. The static pressure rise and the power consumption vary with the density of air ρ_a. The actual density is evaluated according to the the ISO-5801 standard, by measuring the atmospheric pressure P_a, the dry temperature T_{ad} and the wet temperature T_{aw}, from which the partial pressure of the water vapour P_{av} is computed:

$$\rho_a = \frac{P_a - 0.378 P_{av}}{287 T_{ad}} \tag{1}$$

According to the repetition of measurements and simple propagation of uncertainty rules, the relative uncertainty of ρ_a is $\pm 0.3\%$. Please note that all the presented results are rescaled to a reference density $\rho_a = 1.21$ kg.m^{-3}.

Volume flow rate Q_v. As presented previously, the volume flow rate is measured by an ISO-5167 orifice plate at more than $15D$ downstream of the CRS. According to the standard:

$$Q_v = \frac{\alpha \varepsilon \pi d^2}{4} \sqrt{2 \frac{\Delta P_q}{\rho_a}} \tag{2}$$

with ΔP_q the pressure drop measured by a differential pressure transducer. According to the repetition of measurements and to the accuracy of the transducers, the uncertainty of Q_v is $\pm 0.5\%$ at the design flow rate.

Correction for the losses. In order to eliminate the influence of the experimental facilities such as the honeycomb, the driving motor housing and the anti-gyration device, the static pressure drop was measured with both the Front and Rear Rotors removed. Meanwhile, the axial blower at the outlet of the test rig was used to create a flow. Then the correction $Corr$ is modelled as a function of the orifice plate pressure drop ΔP_q. At the design point, the uncertainty of $Corr$ is about $\pm 0.5\%$, which means ± 0.6 Pa.

Static pressure rise ΔP_s. The static pressure rise ΔP_s is the difference between the static pressure downstream of the CRS and the inlet total pressure:

$$\Delta P_s = \Delta P_v + Corr - \frac{1}{2} \rho_a \left(\frac{Q_v}{\pi D^2 / 4} \right)^2, \tag{3}$$

with ΔP_v being measured by the average of 4 pressure taps downstream of the anti-gyration device, with an uncertainty of ± 1 Pa at the design point. The uncertainty of ΔP_s is then ± 4 Pa close to the design flow rate, that is a relative uncertainty of $\pm 1\%$.

Power consumption P_{wt}. The total power consumed by the CRS is defined as:

$$P_{w,t} = P_{w,FR} + P_{w,RR} = \tau_{FR} \omega_{FR} + \tau_{RR} \omega_{RR} \tag{4}$$

with τ the torque of motor, which is measured by the servo-controllers of the two brush-less AC motors and has been calibrated against a rotating torquemeter. It is corrected by the value measured when the rotor is removed from the shaft. The uncertainties of the total power consumption is ± 4.5 W that is 0.8% of the power at the design point.

Static efficiency η_s. The static efficiency is defined as:

$$\eta_s = \frac{\Delta P_s \times Q_v}{P_{w,t}} \tag{5}$$

The relative uncertainty of η_s is $\pm 2.3\%$ (± 1.5 percentage-points at the nominal flow rate).

4 RESULTS AND DISCUSSION

4.1 Overall performance of the three CRS working on design parameters

The static pressure rise and static efficiency as a function of volume flow rate, are presented in Fig. 4, for the three systems. Closed symbols stand for the Front Rotors working alone and open symbols stand for CRS at their θ_C and with $S = 10$ mm. The experimental data and the expected values at the nominal flow rate ($Q_v = 1$ m^3.s^{-1}) are given in Table. 3. Overall, the isolated Front Rotors of each system achieves the predicted values quite well. When coupled to their Rear Rotors to form the Counter-Rotating Systems, the ΔP_s of the three are close to the design point, with at maximum a discrepancy of -11.0% for JW3.

Furthermore, it can be observed from Fig. 4(a) that the characteristics can be divided into 4 regions where the slopes are different:

Region I, $Q_v = [0, 0.38]$. In this region, the volume flow rates are very low. For each configuration, the characteristic curves of the Front Rotors alone and of the Counter-Rotating Systems show similar trend (*i.e.*, flat curves for JW2 and JW2$_{FR}$, significantly negative slopes for JW3 and JW3$_{FR}$).

Region II, $Q_v = [0.38, 0.6]$. In this region, the curves of ΔP_s have relatively high slopes for all the configurations. The slopes for the Front Rotors alone are approximately -277, -113 and -294 Pa.m^{-3}.s for JW1$_{FR}$, JW2$_{FR}$ and JW3$_{FR}$, respectively. The slopes for the CRS are steeper (-606, -537 and -357

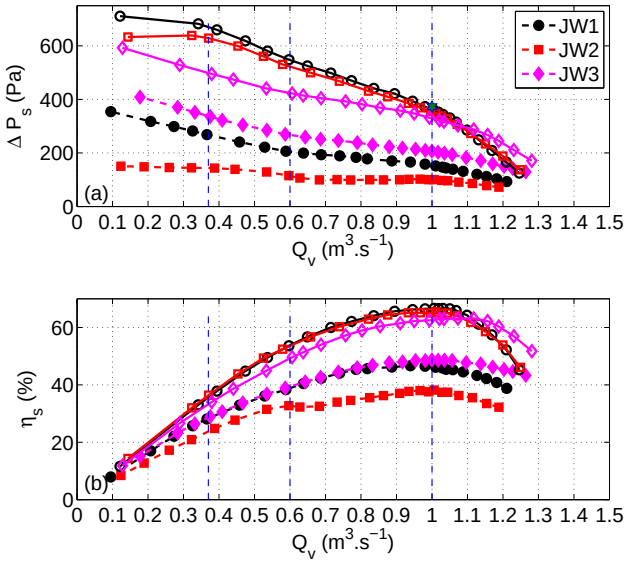

FIGURE 4. Overall performance of four systems: JW1(○), JW2 (□) and JW3 (◊); $JW1_{FR}$ (●), $JW2_{FR}$ (■) and $JW3_{FR}$ (♦), design point,(✡) (a): Static pressure rise ΔP_s *vs.* volumetric flow rate Q_v. (b): Static efficiency η_s *vs.* volumetric flow rate Qv, at $S = 10$ mm.

	FR			CRS		
	Exp (Pa)	*MFT* (Pa)	δ %	*Exp* (Pa)	*C* (Pa)	δ %
JW1	154±2	144	7.0	363±4	373	-2.7
JW2	100±2	96	4.2	353±4	373	-5.4
JW3	207±2	210	-1.4	332±4	373	-11.0

TABLE 3. Comparison of ΔP_s for the three CRS $Q_v = 1$ m^3.s^{-1}, at $S = 10$mm. *Exp*: experimental value, *MFT*: value predicted for the Front Rotor alone, and *C*: design point. The relative difference between the actual and the predicted value is δ.

Pa.m^{-3}.s for JW1, JW2 and JW3). Please note that these values could change rather strongly according to the chosen points. They nevertheless illustrate the trend.

Region III, $Q_v = [0.6, 1]$**.** In this region, of moderate partial flow rates, the curves of ΔP_s have the smallest slopes. The values are roughly -110, 9 and -139 Pa.m^{-3}.s for $JW1_{FR}$, $JW2_{FR}$ and $JW3_{FR}$, respectively. Please note the almost zero or even slightly positive slope of $JW2_{FR}$, that would lead to poor working stability for this fan if it were used alone in an air-loop. For the three CRS, the slopes are increased to -458, -435 and -208 Pa.m^{-3}.s for JW1, JW2 and JW3.

Region IV, $Q_v = [1, 1.3]$**.** In this region of overflow, curves of ΔP_s have the biggest slopes. The values are roughly -282, -133 and -288 Pa.m^{-3}.s for $JW1_{FR}$, $JW2_{FR}$ and $JW3_{FR}$, respectively. Whereas the slopes are increased to -951, -836 and -468 Pa.m^{-3}.s for JW1, JW2 and JW3.

In short, the characteristics of the three CRS are steeper than that of the Front Rotors alone and are always negative on a wide range of partial and over flow rates. This is particularly impressive for the Counter-Rotating System JW2 for which the curve of $JW2_{FR}$ working alone is quite flat. The presence of the Rear Rotors thus contributes to maintain the system stability even at extremely low flow rates in this type of machines. One can finally notice that the best system in terms of static pressure rise is JW1, with an intermediate repartition of the work on the two rotors (60% for $JW1_{FR}$, 40% for $JW1_{RR}$).

FR	η_{sFR} %	CRS	η_{sCRS} %	Gain (η_{sCRS}-η_{sFR})
$JW1_{FR}$	46.3 ± 1.0	JW1	66.6 ± 1.4	20.5
$JW2_{FR}$	38.0 ± 1.0	JW2	65.2 ± 1.4	27.7
$JW3_{FR}$	48.7 ± 1.0	JW3	62.6 ± 1.4	14.6

TABLE 4. Comparison of η_s at design point $Qv = 1$ m^3.s^{-1}

The values of the static efficiencies η_s at the design flow rate are reported in Tab. 4. The three CRS are very efficient, the typical peak efficiency of a traditional rotor-stator stage being of the order of 55% according to Ref. [8], and up to 60% for exceptional stages. For a single rotor stage, the typical static efficiency is 50%, up to 55% (see also Refs. [7–9]). In view of this, the Counter-Rotating System is a promising solution for the designers who seek for high static efficiency turbomachines.

4.2 Influence of the axial distance S on the performances of CRS at $\theta = \theta_C$ and $Q_v = 1$ m^3.s^{-1}

The variations of ΔP_s and η_s with the axial distance S between the Front Rotor and the Rear Rotor at the design flow rate are plotted in Fig. 5 for the three CRS working on their nominal speed ratios $\theta = \theta_c$. As a reference, the values for Front Rotors alone are plotted at $S = 0$ with closed symbols. The values decrease monotonically with S for the three CRS, contrary to the results observed by Pundhir & Sharma [10] on a transonic case where an optimum in distance was found. In the present

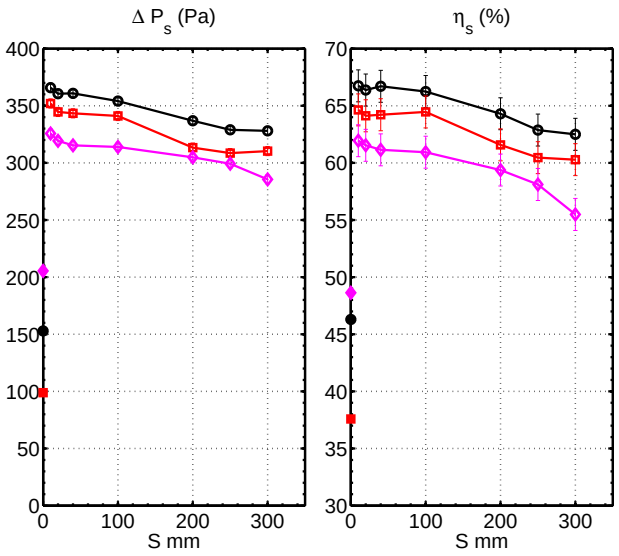

FIGURE 5. η_s of JW1 (○), JW2 (□) and JW3(◊) at $S = 10$, 20, 40, 100, 200, 250, 300 mm and Rront Rotor alone($S = 0$, filled symbols) at design point $Q_v = 1\text{m}^3.\text{s}^{-1}$, $\theta = \theta_c$

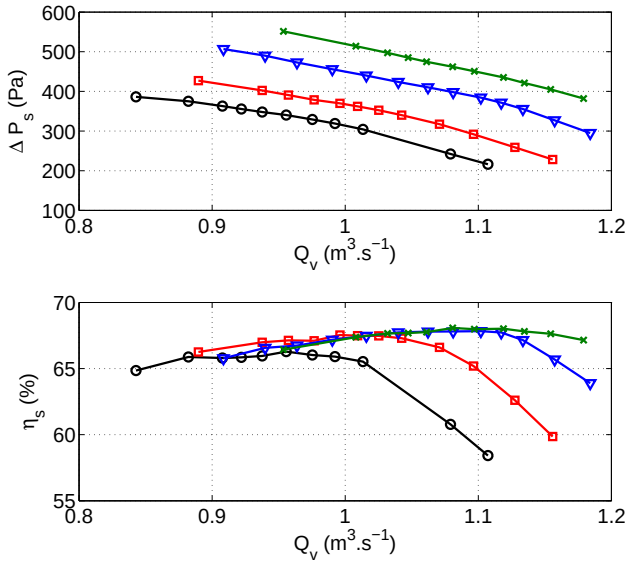

FIGURE 6. Static efficiency of stage JW1 at $Qv = 1$ m^3.s^{-1}, $S =$ 10 mm, $\theta/\theta_c = [0.9$ (○), $1,0$(□), 1.15(▽), 1.25(×)], $\theta_c = 0.96$.

case, the static pressure rise declines rapidly as $S < 40$ mm, then decreases slightly as $S \in [40, 100]$ mm before decreasing significantly as $S \in [100, 300]$ mm. When the distance is small, on the one hand the Rear Rotor recovers more swirl energy downstream of the Front Rotor. But on the other hand, the power consumption of the Front Rotor slightly increases. Nevertheless, in our case the relative increase in static pressure is greater than the relative increase in power consumption, which leads firstly, to a monotonic variation of the efficiency and secondly, to a stronger effect of the distance on the static pressure rise than on the efficiency.

4.3 Inluence of speed ratio θ on the performances of CRS

4.3.1 JW1 As illustrated in Fig. 6, the nominal flow rate is shifted towards higher flow rates as θ increases. In this section, the maximum static efficiency $\eta_{s,max}$ is presented and analysed instead of η_s at $Q_v = 1$ m^3.s^{-1}.

For JW1, the performances are improved up to a maximum static efficiency of 68% when θ is increased from $0.9\theta_c$ to $1.25\theta_c$. This feature has also been observed for the system used in Ref. [4].

Due to the limitation of the rotational speed of the motors at maximum 3000 rpm, it is difficult to get higher θ and at the same time keep $N_{FR} = 2300$ rpm. One solution to get higher speed ratios is to decrease the N_{FR}. Figure. 7 presents the $\eta_{s,max}$ as a function of θ/θ_c at $N_{FR} = 2300$ rpm and $N_{FR} = 1400$ rpm. Overall, the two curves have the same trend but are shifted by about 2 percentage points. This discrepancy could be explained as an effect of the Reynold's number Re. Lower Re induces larger losses in the flow which deteriorates the efficiency.

The Reynold's number based on the inlet relative velocity W and on the chord length L_{chord} at mid-span, $Re = \frac{\rho_a W L_{chord}}{\mu}$ is of the order of $Re \approx 1.2 \times 10^5$ for JW1 at $N_{FR} = 2300$ rpm, and $Re \approx 7.7 \times 10^4$ at $N_{FR} = 1400$ rpm. Aside from the influence of Re, it can be seen in Fig. 7 that $\eta_{s,max}$ reaches a peak value for $\theta \approx 1.15\theta_c$ and decreases for $\theta \gtrsim 1.2\theta_c$.

4.3.2 JW1, JW2 and JW3 Figure. 8 gives the trend of the variation of the maximum static efficiency $\eta_{s,max}$ with the speed ratio for the three CRS. Favourably, all the CRS could maintain the $\eta_{s,max}$ beyond 60% even working at far from design condition and low rotational speed. This shows that a CRS does not only improve the efficiency to a high level, but is also robust at maintaining its high performance at various off-set conditions.

Additionally, it is obvious that $\eta_{s,max}$ increases significantly as θ is increased to θ_c, then continues to rise slightly as θ reaches $1.2\theta_c$, for all the three CRS. Nevertheless, the maximum efficiency drops down moderately as $\theta > 1.2\theta_c$ for JW1 and JW2, but on the contrary, for JW3 it continues to increase untill $\theta = 1.6\theta_c$. This could own to the increased contribution of the Rear Rotor for this system.

4.4 Influence of both the axial distance S and θ on the performances of JW1

In the previous analysis, the influence of S and θ on the performances have been investigated separately. The figure. 9

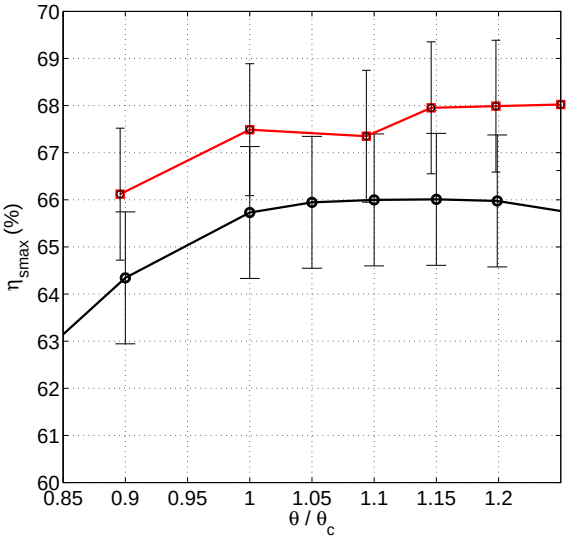

FIGURE 7. Maximum static efficiency *vs.* θ. Stage JW1, at $N_{FR} =$ 1400 rpm (○), $N_{FR} = 2300$ rpm (□), $S = 10$ mm.

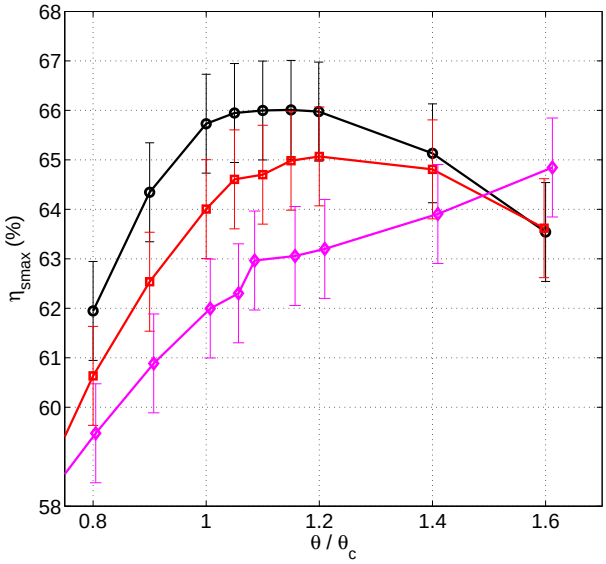

FIGURE 8. Maximum static efficiency *vs.* θ. Stage JW1, $N_{FR} =$ 1400 rpm, $Re \approx 7.7 \times 10^4$ (○). JW2, $N_{FR} = 1100$ rpm, $Re \approx 5.2 \times 10^4$ (□). JW3, $N_{FR} = 1600$ rpm, $Re \approx 8.0 \times 10^4$ (◇).

demonstrates that the identified trend of the maximum static efficiency increase as θ increases is similar for all the axial distance in $[10, 200]$ mm.

4.5 Analysis of the wall pressure fluctuations

The wall pressure fluctuations are measured by a microphone situated at a distance $Z_p = 5$ mm downstream of the Front Rotor (see Fig. 1). The power spectral density (PSD) of these fluctuations for the three systems working at their design conditions and with $S = 10$ mm are plotted in the Figs. 10 to 12. For each system, two flow rates have been studied: the design flow rate $Q_v = 1$ m^3.s^{-1} and a partial flow rate $Q_v = 0.6$ m^3.s^{-1}. One can notice the presence of several peaks in the spectra. These peaks can be divided into three types: those that correspond to

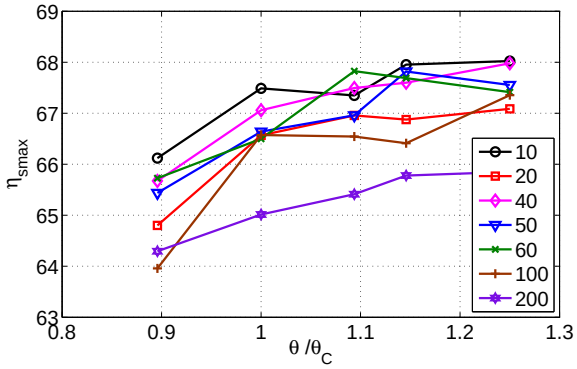

FIGURE 9. Maximum Static efficiency of the stage JW1 at $N_{FR} =$ 2300 rpm, *vs.* θ/θ_c for $S = 10$ mm (○), $S = 20$ mm (□), $S = 40$ mm (◇), $S = 50$ mm (▽), $S = 60$ mm (×),$S = 100$ mm (+) and $S = 200$ mm (✡).

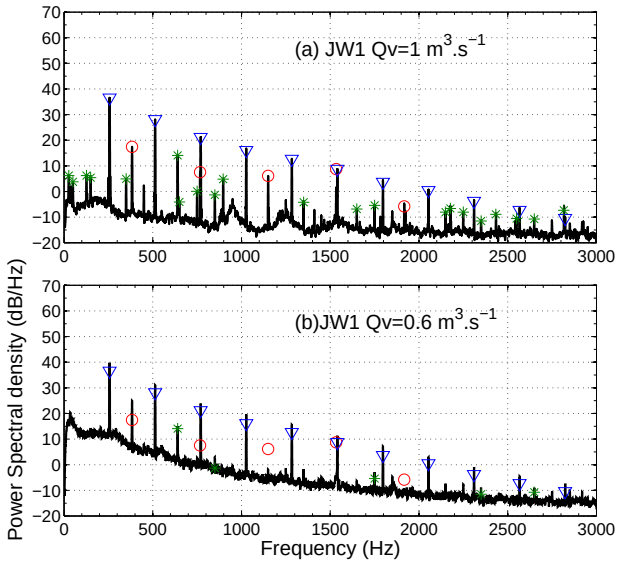

FIGURE 10. PSD of the wall pressure fluctuations measured at $Z_p =$ 5 mm, for JW1 at $N = 2300 - 2200$ rpm and $S = 10$mm, (a)$Q_v =$ 1 m^3.s^{-1}; (b)$Q_v = 0.6$ m^3.s^{-1}. (○): $mf_{bpf,FR}$, (▽): $nf_{bpf,RR}$, and (∗): $mf_{bpf,FR} + nf_{bpf,RR}$ with $m \neq 0$ and $n \neq 0$.

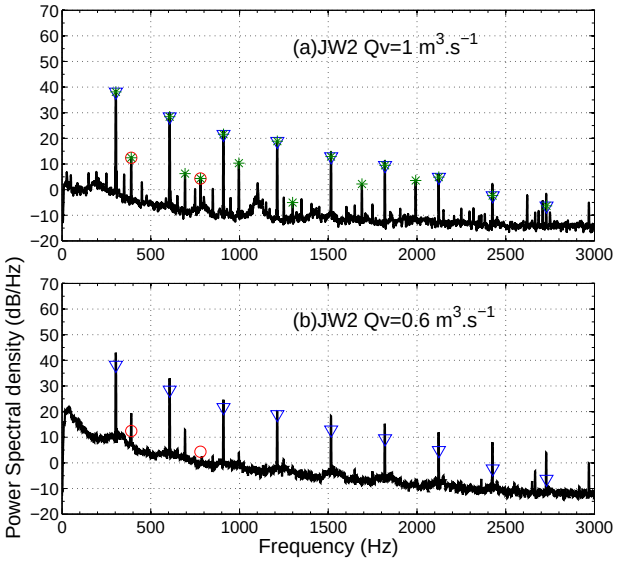

FIGURE 11. PSD of the wall pressure fluctuations measured at $Z_p =$ 5 mm, for JW2 at $N = 1800 - 2600$ rpm and $S = 10$mm, (a)$Q_v =$ 1 m^3.s^{-1}; (b)$Q_v = 0.6$ m^3.s^{-1}. ($\circ$): $mf_{bpf,FR}$, ($\triangledown$): $nf_{bpf,RR}$, and ($*$): $mf_{bpf,FR} + nf_{bpf,RR}$ with $m \neq 0$ and $n \neq 0$.

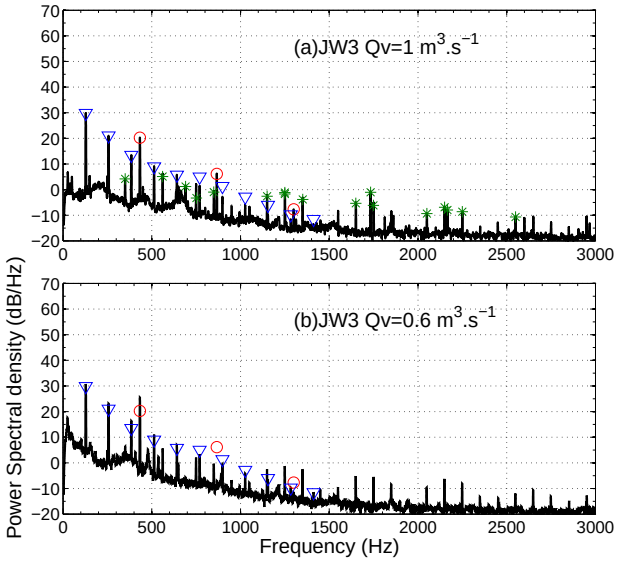

FIGURE 12. PSD of the wall pressure fluctuations measured at $Z_p =$ 5 mm, for JW3 at $N = 2600 - 1100$ rpm and $S = 10$mm, (a)$Q_v =$ 1 m^3.s^{-1}; (b)$Q_v = 0.6$ m^3.s^{-1}. ($\circ$): $mf_{bpf,FR}$, ($\triangledown$): $nf_{bpf,RR}$, and ($*$): $mf_{bpf,FR} + nf_{bpf,RR}$ with $m \neq 0$ and $n \neq 0$.

the blade passing frequency of the Front Rotor ($f_{bpf,FR}$) and its harmonics are marked with $\circ$, while the peaks corresponding to the Rear Rotor blade passing frequency ($f_{bpf,RR}$) are marked with $\triangledown$ and finally, the interactions frequencies corresponding to combinations of the Front and Rear Rotor blade passing frequencies are marked with $*$. As a reference, the amplitudes of the symbols in the Figs. 10 to 12(b) are kept the same as in the Figs. 10 to 12(a), in order to compare the changes between $Q_v = 1$ m^3.s^{-1} and $Q_v = 0.6$ m^3.s^{-1}.

Several common features can be noticed. Firstly, the amplitudes of the peaks corresponding to $f_{bpf,RR}$ and its harmonics are always significantly higher than that of $f_{bpf,FR}$. The influence of the Rear Rotor propagates upstream (potential effect) and is stronger than that of the Front Rotor (usually attributed to the wakes of the blades). Then, one can notice that the two rotors are in strong non-linear interaction at the design volume flow rate. However, for $Q_v = 0.6$ m^3.s^{-1}, the peaks corresponding to the interactions are dramatically attenuated, and in contrast, the amplitudes corresponding to both $f_{bpf,FR}$ and $f_{bpf,RR}$ are increased.

In order to compare now the three systems, the amplitude of the peaks corresponding to $f_{bpf,FR}$ and $f_{bpf,RR}$ are reported in Tab. 5 for the design volume flow rate. JW2 has the highest amplitude for $f_{bpf,RR}$ and the lowest for $f_{bpf,FR}$ among the three CRS. This is consistent with the ratio of rotational speeds. Finally, one can notice a correlation between the levels and the rotation rates of the rotors. The total level of the pressure fluctuations is thus obviously the lowest for JW3, and is almost similar for JW1 and JW2 when the sums of the two rotation rates are of the same order of magnitude.

	N_{CFR}/N_{CRR} (rpm)	PSD_{FR} (dB/Hz)	PSD_{RR} (dB/Hz)	Std(p') (dB)
JW1	2300/2200	17.4	36.5	40.9
JW2	1800/2600	12.6	38.5	42.9
JW3	2600/1100	20.2	29.8	35.1

TABLE 5. The amplitude of the dominate frequency corresponded to $f_{bpf,FR}$ and $f_{bpf,RR}$, for JW1, JW2 and JW3, at $Q_v = 1$ m^3.s^{-1}. Std(p') represents the power of the total signal.

5 CONCLUSIONS

Three subsonic Counter-Rotating axial-flow fans Systems (JW1, JW2 and JW3) have been designed. The design objective is to reach the same design point with various distributions of the work and rotation rates between the rotors. Series of experiments have been conducted to explore the influence of design parameters on the overall performances of these CRS. It can be concluded that:

1. All three CRS can achieve the design point, with maximum 11% of discrepancy. Besides, the best static efficiency is

very high —above 65%for the three systems. The design method is thus satisfying for a pre-study, but may be improved, especially by including an analysis of the total system and developing an equation of the radial equilibrium for the whole stage.

2. The performance map shows that over the major part of operating range, with the contribution of the Rear Rotor, the slopes of the CRS are always negative, which stands for good working stability of this kind of axial turbomachine.
3. Short axial distances S are favourable for maintaining high performance. The results show that the ΔP_s and η_s diminished monotonically with the axial distance increase, in other words no optimum in distance is found contrary to what was reported for highly compressible CRS [10].
4. The maximum efficiency $\eta_{s,max}$ could be steadily increased as the speed ratio varies in $[1,1.2]\theta_C$. Furthermore, $\eta_{s,max}$ could be kept above 60% for $\theta \pm [0.8,1.6]\theta_C$.
5. The power spectral densities of the wall pressure fluctuations between the rotors show that the dominant frequency corresponds to the blade passing frequency of the Rear Rotor and that the zone between the two counter-rotating rotors is a zone of high interactions between instationary flows. This feature should also be taken into account for better design and optimization.

REFERENCES

[1] Cho, L., Choi, H., Lee, S., and Cho, J., 2009. "Numerical and experimental analyses for the aerodynamic design of high performance counter-rotating axial flow fans". In Proc. ASME 2009 Fluids Engineering Division Summer Meeting, Colorado, USA, pp. FEDSM2009–78507.

[2] Shigemitsu, T., Furukawa, A., Watanabe, S., Okuma, K., and Fukutomi, J., 2009. "Internal flow measurement with ldv at design point of contra-rotating axial flow pump". *J. Fluid Sci. and Technology,* ***4***, pp. 723–734.

[3] Moroz, L., Pagur, P., Govorushchenko, Y., and Grebennik, K., 2009. "Comparison of counter-rotating and traditional axial aircraft low-pressure turbines integral and detailed performances". In Int. Symp. on Heat Transfer in Gas Turbine Systems, Antalya, Turkey.

[4] Nouri, H., Danlos, A., Ravelet, F., Bakir, F., and Sarraf, C., 2013. "Experimental study of the instationary flow between two ducted counter-rotating rotors". *J. Eng. Gas Turbines Power,* ***135***, p. 022601.

[5] Noguera, R., Rey, R., Massouh, F., Bakir, F., and Kouidri, S., 1993. "Design and analysis of axial pumps". In Proc. ASME 1993 Fluids Engineering, Second Pumping Machinery Symposium, Washington USA, pp. 95–111.

[6] Vad, J., 2012. "Forward blade sweep applied to low-speed axial fan rotors of controlled vortex design: An overview". *J. Eng. Gas Turbines Power,* ***135***, p. 012601.

[7] Sarraf, C., Nouri, H., Ravelet, F., and Bakir, F., 2011. "Experimental study of blade thickness effects on the overall and local performances of a controlled vortex designed axial-flow fan". *Exp. Thermal and Fluid Science,* ***35***, pp. 684–693.

[8] Bakir, F., and Moreau, S., 2002. "Efficient stator designed for automotive engine cooling fan systems.". In Proceedings of the ASME 2002 Fluids Engineering Division Summer Meeting, pp. FEDSM02–31318.

[9] Yen, S. C., and Lin, F. T., 2006. "Exit flow field and performance of axial flow fans". *J. Fluids Eng.,* ***128***, pp. 332–340.

[10] Pundhir, D., and Sharma, P., 1992. "A study of aerodynamic performance of a contra-rotating axial compressor stage". *Defence Science Journal,* ***42***, pp. 191–199.